Published in final edited form as:
Theor Chem Acc. 2015 December ; 134(12): . doi:10.1007/s00214-015-1753-0.

Virtual eyes for technology and cultural heritage: toward computational strategy for new and old indigo-based dyes

Vincenzo Barone,
Scuola Normale Superiore di Pisa Piazza dei Cavalieri 7, I-56126 Pisa, Italy

Malgorzata Biczysko,
Physics Department, and International Centre for Quantum and Molecular Structures, Shanghai University, 99 Shangda Road, Shanghai, 200444 China

Camille Latouche, and
Scuola Normale Superiore di Pisa Piazza dei Cavalieri 7, I-56126 Pisa, Italy

Andrea Pasti
Scuola Normale Superiore di Pisa Piazza dei Cavalieri 7, I-56126 Pisa, Italy

Abstract

A cost-effective, robust, and reliable computational strategy is applied to simulate peak positions and band-shapes of UV-vis spectra together with the dye colours perceived by human eyes. The features of our virtual multifrequency spectrometer (VMS) relevant to this topic are sketched with special focus on the selection of density functional, vibronic model, and solvent description. Furthermore, the new VMS-Draw graphical user interface (GUI) is employed for user-friendly pre- and post-processing of the computed data. The family of indigo dyes is used as case study in view of their continued use in the field of cultural heritage, together with new promising applications for photonics and sustainable energy. After assessment of different simplified models employed in previous studies, the role of several substituents and of dimerization in tuning the colour and spectral features are analyzed in detail by means of both accurate computations and interpretative models. The results are in remarkable agreement with experiment and allow to rationalize the behaviour of this class of dyes.

Keywords

indigoids; quantum-mechanical calculations; TD-DFT; electronic spectra line-shapes

1 Introduction

After the era of electronics, we are now witnessing the beginning of the photonics era in which attention is being shifted from electrons to photons. Together with experimental challenges, this new adventure calls for renewed interest to quantum mechanical (QM) methods able to couple reliability and feasibility for prediction and interpretation of light-

Paper dedicated to the UNESCO International Year of Light and Light-based Technologies (IYL 2015). TCA special Issue on Health Energy from the Sun: a Computational Perspective.

Europe PMC Funders Author Manuscripts

matter interactions involving large molecular systems in their natural environments. The new scenario goes well beyond conventional spectroscopic studies to include a number of multidisciplinary research fields including life- and material-science[1–15], with special emphasis for 'green processes' like e.g. photovoltaics[16–18] and artificial photosynthesis[5, 6, 19, 20]. In the last few years also cultural heritage, which is the focus of the present study, has been involved in these developments[21–26] since exploration of different spectral ranges is mandatory for the development, validation, and systematic application of new integrated tools improving the current status of analysis, conservation, and restoration strategies. Here, 'old' spectroscopic phenomena like UV-vis absorption leading to different colours of pigments still accompany the most recent non-linear vibrational and electronic spectroscopies providing data of unprecedented accuracy and sensitivity.

All those issues raise new and more challenging tasks for computational spectroscopy, which is becoming increasingly important as an invaluable tool to assist and sometimes guide experimental studies[1, 27–29] and to predict properties of new not-yet synthesised materials[8, 12]. As a matter of fact, direct interpretation of experimental results in terms of structural, dynamical, and environmental effects is by no means trivial and is significantly enhanced by computational studies provided that the latter couple reliability and feasibility for the large systems of current scientific and technological relevance in their natural environments. In the last years the study of medium and large-size molecules has been revolutionized by the development of methods based on the density functional theory (DFT) and its time-dependent extension (TD-DFT)[30, 31] which are nowadays providing remarkably accurate results at least for low-lying valence excited states. The range of application of these techniques is being constantly increased thanks to ongoing efforts to solve some well-known shortcomings (e.g., charge transfer states, double excitations, etc.) [32, 34]. In particular, the development of effective analytic gradients[35, 36] and, very recently, of analytic Hessians[37, 38], is allowing a full characterization of excited electronic states.

In this context, moving from the standard practice of extracting numerical data from experiment to be compared with quantum mechanical results toward the direct comparison between recorded and computed spectra would strongly reduce any arbitrariness and allow a proper account of the information hidden behind both positions and shapes of spectral bands[39–43]. In particular, the convolution of vertical (or adiabatic) excitation energies by phenomenological distribution functions completely neglects the vibrational structure present in experimental UV-vis spectra. As a consequence, several peaks present in high-resolution spectra cannot be correctly interpreted and, even worse, the asymmetry and relative intensities of most bands in low-resolution spectra cannot be often reproduced. Vibronic effects are also of paramount relevance in the context of energy transfer and conversion, e.g. in photosystem complexes[44–47]. In the context of dyes and pigments proper account of the vibrational structure is crucial for the prediction of the colour of the compounds, since the band shape is directly responsible for the color perceived by the human eye [26, 48]. Recently direct vis-à-vis comparison between simulated and computed spectra has been greatly facilitated by the development of user friendly computational models for vibronic computations[49–57] and their implementation into widely used computational packages[50–53]. In particular, in our group we are actively developing a

virtual multi-frequency spectrometer (VMS),[39, 58] which consists of a comprehensive computational part providing access to the latest developments of computational spectroscopy (VMS-comp)[50–52, 59–62] and a powerful graphical interface (VMS-draw) [63], the latter being able to pre- and post-processing the data, as well as to compare them directly with the experimental spectra. The sections of VMS in charge of electronic spectroscopy, within the time-independent (TI)[50, 51, 64] or time-dependent (TD)[52, 65] routes, have been employed in the present study.

The computational machinery will be presented and applied to a comprehensive analysis and interpretation of the most interesting structural and spectroscopic features of a family of well known dyes, namely indigo derivatives and new indigo-based materials with special focus on the relationship between structure, substituents, and colour changes, which is mediated by the corresponding modification of positions and shapes of visible spectra bands. Indigo is one of the oldest dyes used by mankind[66–68], starting from its well documented employment as a blue dyestuff in the pre-Vedic period in India where *Indigofera tinctoria L.* was its more common source, and continuing till the development of organic synthesis of this compound in the XIX century from isatin[69]. Indigo is also known as the chromophore of Maya Blue, a precolombian pigment prepared by precipitating indigo on a white clay, usually palygorskite. Maya Blue was used in wall paintings and ceramics and it has been widely studied due to its unusual stability and hue of color[23, 70]. Indigo and its derivatives have been valued for their bright colours and photochemical stability over the years and are within the most studied dyes from both experimental and theoretical points of view (see for example References [21, 25, 71–78] and references therein). The current consumption of indigo is largely affected by the popularity of blue jeans, which are dyed with indigo, but together their use as colorants, indigo derivatives and oligomers received recently increased interest also in other technological fields[79]. Applications of ’old indigo’ as building block in novel ’smart materials’ include organic photovoltaic devices based on conjugated polymers containing indigo unit in the main chain[80, 81], indigo derivatives showing non-linear optical properties[82] or extended indigo semiconductors for organic electronic applications, demonstrating impressive stability under ambient conditions[83].

The renaissance of indigo-based dyes toward the design of molecules and macro-molecular systems with purposely tailored structure and function, for advanced technologies[84], raises a number of questions about the development of effective computational models allowing reliable prediction of their micro- and macroscopic properties. This makes the ’indigo family’ an ideal case study for advanced computational spectroscopy approaches and prompted us to perform a comprehensive analysis of several indigo models, derivatives, and oligomers considering not only the electronic properties in the excited electronic states, but also the environmental and vibronic effects tuning the spectra line shape and the perceived colour. Together with specific reference to indigo, we will try to provide also general guidelines about the application of the VMS tool for accompanying experimental studies with special reference to cultural heritage problems.

2 Computational Details

Quantum mechanical (QM) calculations have been performed by methods rooted into the density functional theory (DFT) and its time-dependent extension (TD-DFT) [30, 31, 36], employing B3LYP[85], CAM-B3LYP (CAM) [86], M06-2X[87, 88], ω-B97XD[89] and PBE1PBE (PBE0) [90] functionals, in conjunction with the SNSD double-ζ basis set[91–93] including Stuttgart-Dresden core pseudopotentials[94, 95] for bromine. Bulk solvent effects have been taken into account by means of Polarizable Continuum Model[96] within its C-PCM (Conductor-like PCM) [97] formulation, with the default parameters of chloroform.

All ground state geometries have been optimized by all the used functional and the resulting planar structures have been confirmed as minima on the potential energy surface (PES). These geometries have been used to simulate the UV/vis spectra either by vertical excitation energies (VE) or vibronic, Vertical Gradient (VG)[51, 64] models. For selected compounds, equilibrium geometry structures and vibrational frequencies in the first excited electronic state have been also computed at the TD-B3LYP/SNSD(CPCM) level, in all cases leading to the true minimum on the excited state PES. This information allowed us to perform vibronic computations with the Adiabatic Hessian (AH) [50, 51, 64] model. The adiabatic TD-DFT energies (AE) have been computed with different functionals, on the ground and excited state equilibrium structures optimized at the (TD-)B3LYP/SNSD(CPCM) level and applied to define the position of the AH spectra on the absolute energy scale. The AH spectra are labelled in the Figures and in the Tables according to the method used to compute AE.

Concerning spectra simulations, vertical models (vertical gradient (VG) or Vertical Hessian (VH)), employ the same reference geometry for both initial and final state (the equilibrium geometry of the initial state for absorption spectra), i.e. focus on the region corresponding to the most intense transitions, while the equilibrium geometry of the final state is extrapolated. Within adiabatic models (Adiabatic Shift (AS) or adiabatic Hessian (AH)), the focus is on the equilibrium struc-ture of the final state, and the spectral features close to the 0-0 transition, i.e., the transition be-tween the vibrational ground states of two electronic states. For semi-rigid systems both types of approaches provide similar results, while anharmonic effects enhance the differences be-tween them. It is noteworthy, that computation times are comparable concerning the vibronic part for all models, thanks to the strong optimization of our code, but AH (and VH) approaches require Hessians of excited states, which are very computationally intensive. Furthermore, if the geometries of initial and final states are significantly different, the VG model (which is identical for different sets of coordinates) is often more stable, while AH computations might be better suited for internal coordinate approaches (see for instance Ref. [98] and references therein). Finally, the VG approach represents a feasible route to simulation of absorption spectra in large energy ranges encompassing several excited electronic states.

For the indigo dimer the ground state structure optimisations have been performed with the standard B3LYP functional and its dispersion corrected version, using the Grimme's model, B3LYP-D3[99, 100], in both cases including solvent effects by means of the CPCM. The latter structure has been used to simulate electronic spectra within the VG model with forces

in the excited state computed at the TD-B3LYP-D3/SNSD(CPCM) level. In all cases non-equilibrium solvent effects on the vertical excitation energies have been computed with the linear response LR-PCM/TD-DFT approach[36, 101], suitable to describe the absorption spectrum in solution due to the different time scales of the electronic and nuclear effects.

For the comparison with broad features of the reference experimental absorption spectra the theoretical stick spectra including all relevant vibronic transitions have been convoluted by means of Gaussian distribution functions with Half-Width at Half-Maximum (HWHM) equal to 750 cm^{-1}. The simulated electronic spectrum in a 250-800 nm range has been obtained by adding the contributions from all bright electronic transitions. The colour of compounds has been evaluated considering its spectrum in the 380-780 nm (vis) range. The International Commission on Illumination (CIE) colour coordinates have been obtained calculating the spectral overlap with the standard CIE Red, Green and Blue colour matching functions [102], and then converted to RGB colour model.

All computations were performed using the GAUSSIAN09 package[103]. A new graphical user interface (VMS-Draw)[63] was used to analyze in detail the outcome of vibronic computations, compute RGB parameters and plot electronic spectra.

3 Results and Discussion

3.1 Structural and spectroscopic properties of Indigo and its reduced models

The properties of the first bright excited electronic state of indigoid dyes are associated with the presence of the donor groups such as -NH- and -S- and acceptor ones such as C=O. Over the years several reduced molecular models have been proposed in order to describe properties of indigo and its derivatives (see the Scheme 1), starting from the so-called 'H-chromophore' (**M0**)[71, 72], toward the 'half-indigo' isatin (**M1**) and bispyrroleindigo (**M2**), with the last recently applied in state-of-the-art studies on the photostability[78] and nonadiabatic dynamics[104] of indigo. Although these truncated models have been already compared with the indigo molecule (**1**) considering mainly electronic properties and UV-vis spectra within the vertical excitation framework[74, 76], in the present work we will also address the effects of nuclear degrees of freedom and their relative changes upon the electronic excitation on the spectroscopic properties.

We first discuss the composition of the frontier Molecular Orbitals (MOs) of compounds **M1**, **M2** and **1**. The plots of frontier MOs, obtained at the B3LYP/SNSD level are presented in Figure 1. We note that all functionals considered in this work show equivalent results as far as an analysis of MOs is concerned. For **M1** the HOMO-1 is mainly localized on the carbonyls whereas the HOMO has a strong phenyl moiety character with a bonding behavior and a non-negligible contributions of nitrogen. The LUMO is mainly localized on the carbonyls and on the phenyl whereas the LUMO+1 shows a strong phenyl character. These MOs of **M1** are substantially different from those of compounds **M2** and **1**, which in turn have their frontier orbitals quite similar to each other. The HOMOs of both **M2** and **1** compounds are strongly delocalized and have a strong participation of the double C=C bond and of the nitrogen atoms, while **M2** shows also larger localization on the carbonyls. Their LUMOs are also very similar with a strong participation of both carbonyls and double C=C

bonds. Moreover, the HOMO and LUMO of **1** are also partially localized over the phenyl moiety, which seems to increase for the HOMO-1 and LUMO+1.

These differences in MOs composition and energies are reflected in the vertical excitation energies, reported in Table 1. The first bright excited electronic state is essentially due to the HOMO-LUMO transition with vertical excitation energies computed at the TD-PBE0/SNSD/CPCM level of 413 nm, 490 nm and 581 nm for **M1**, **M2** and **1**, respectively. For **M1** the MOs composition shows that the HOMO-LUMO transition involves charge transfer from the nitrogen lone pair and the phenyl moiety to the carbonyls, in line with general donor-acceptor characterisation of indigoid chromophores. The charge transfer associated with **M2** and **1** can be related to increase of electron density on carbonyls and on the C_2-C_3 bonds (see Figure 2), as a result the electronic transition is mainly localized over the 'H-chromophore' unit, but in **1** there are also non-negligible contribution on the phenyl moieties, in analogy to **M1**. It is clear that both reduced models are not able to reproduce the absorption maximum of indigo. These differences can be associated with two different reasons: **M1** simply lacks the H-chromophore system, while for the **M2** (showing smaller discrepancy) the fundamental unit is present but 'more conjugation' with the benzylic condensed rings is needed to lower the energy of the HOMO-LUMO transition to give the typical blue colour of indigo.

The differences between **M2** and **1** are further enhanced going beyond vertical excitation model, i.e. concerning equilibrium structures and properties in the first excited electronic state, which are presented in Figure 2, with selected parameters listed in Table 2. Indigo preserves its high C_{2h} symmetry both in the ground and excited state, while bispyrroleindigo lowers its symmetry to C_s mainly because of an in-plane twisting along the C_2=C_2' double bond of the two pyrrole subunits, which leads to the shortening of one O · · ·H hydrogen bonding distance and elongation of another one, from about 2.33 Å to 1.97 Å and 2.70 Å respectively. Moreover the adiabatic electronic transition in the first excited state of bispyrroleindigo is mainly localized at only one of the two pyrrole subunits while for the indigo both vertical and adiabatic (geomS_0 and geomS1 in Figure 2) frameworks yield the transition delocalized over the whole molecule retaining the symmetry of the ground state. These differences can be attributed to the significantly higher rigidity of **1** imposed by the condensed benzylic rings, with respect to the reduced model, which is reflected by significantly larger variation of geometry parameters for the latter. The main point of this observation is that truncated model is not sufficient to describe indigo from a structural point of view.

The electronic and structural effects are further reflected in the vibronic spectra computed within vertical (VG) and adiabatic (AH) models for **M1**, **M2** and **1**, presented in Figure 3, where rather small value of HWHM have been adopted in order to highlight effects masked by the large broadening of experimental transitions in solution. As expected, both vertical and adiabatic approaches give very similar results, and are able to simulate correctly the absorption spectra of indigo, while for smaller truncated molecules such as bispyrroleindigo there are large discrepancies between both methodologies, in line with significant changes of structural and vibrational properties of **M2** upon electronic excitation. These effects can be quantified by an analysis of shift vectors (**K**), closely-related to Huang-Rhys (HR)

factors[105](the squares of the components of the excited state gradient normalized with respect to the corresponding initial-state vibrational frequency) and Duschinsky matrices (**J**) of **M2** and **1**. In the present case, there is no substantial mode mixing (**J** matrices are nearly diagonal), so that the differences between VG and AH models can be attributed to the geometry changes along normal modes accompanying electronic excitation. Figure 4 reports Huang-Rhys factors computed within VG and AH models, which are nearly identical for **1** and reflect significant changes for **M2**. It is noteworthy that the HR factors computed at the VG level are significantly larger for **M2** than for **1**, indicating that relatively cheap VG computations can be used to asses qualitatively geometry changes in excited electronic states, without performing computationally expensive geometry optimizations, which are possibly further complicated by crossings between different excited states. Moreover, for **1**, all significant vibronic contributions to the electronic spectra line-shape are related to the in-plane normal modes, which preserve molecular symmetry, while the most intense vibronic transitions of **M2** show 'twisted' character (see Figure 5). The larger rigidity of **1** suggest that the trans-cis photoisomerization via the twisting of the central C=C, excluded for **M2**, is even less probable for indigo, confirming that it is unlikely to play a role in its photochemistry[78]. However, in more general terms, different nuclear motion effects found for **1** and **M2** might lead to diverse photochemical behaviour of two compounds. An example is represented by excited state intramolecular proton transfer (ESIPT) between adjacent N-H and C=O groups in the first bright excited state observed for indigo and bispyrroleindigo[78]. The electron density difference (ELD) plots in Figure 2 indicate that for both indigo and bispyrroleindigo nitrogen atoms become more 'acidic' due to the electron transfer toward carbonyl groups, that become more 'basic', so facilitating a proton transfer. However, the analysis of structural parameters do not show significant changes in the O-H-N region for indigo, while for **M2** the twist along double C_2=C_2' bond leads to the shortening of the distance between oxygen atom of one subunit and the hydrogen atom bound to N of the other subunit along with the angle N-H-O' deformation, so the two hydrogen-bonds become non-equivalent, in line with the barrier-less single proton transfer (SPT) reaction found for **M2**[78]. On the contrary, two distinct minima with similar energies corresponding to the keto form and the mono-enol form have been found for **1**, showing again differences between these two compounds. Finally, we conclude that truncated indigo models, from the simplest 'H-chromophore' toward more extended **M1** and **M2** might not be adequate for the studies of spectroscopic and photochemical properties of indigo and its derivatives, as both the main chromophoric unit and the enhanced conjugated π structure are required to properly account for its electronic and nuclear properties. In more general terms, vibronic effects should not be overlooked in the understanding and prediction of photochemical and photophysical properties of chromophoric systems, suggesting new routes toward the development of reliable computational protocols aimed to the rational design of novel indigo-derived dyes.

3.2 UV-vis spectra and colour prediction of indigo derivatives

In order to establish a robust methodology applicable to the indigo derivatives, the spectroscopic properties of **1** have been computed with different functionals and considering both the basic VE approach and different vibronic (VG, AH) models. We first note that the bulk solvent effects described at the LR-TD-DFT/CPCM level lead for all functionals to

non-negligible (0.13-0.17 eV, about 25-45 nm) red-shifts with respect to the gas phase computations for the first bright electronic transition of **1**; therefore only computations in solution will be discussed in the following. From the absorption maxima reported in Table 1 one can see that B3LYP (599 nm) and PBE0 (580 nm) functionals led to the best agreement between the energy of the first allowed transition (first bright one) and the experimental data (604 nm) within VE approach, while recently developed functionals, such as CAM-B3LYP (524 nm), M06-2X (524 nm) and ω-B97XD (522 nm) underestimate the λ_{max} of the observed transition. The good performances of the B3LYP and PBE0 functionals is in line with the results of an extended benchmark of TD-DFT VEs for indigoid dyes[77], whereas the M06-2X and ω-B97XD functionals were not included in the previous study. However, it is well documented that whenever charge-transfer transitions are not involved, global hybrid functionals without too many parameters often perform a better job than their long-range corrected or heavily parametrized counterparts, at least for the lowest valence excited electronic states[32–34]. Once vibronic effects are included by VG or AH models, the computed absorption wavelengths increase in all cases by about 20 nm, so the B3LYP and PBE0 functionals show again the best agreement with experiment, within about 10 nm. For the other functionals, the mismatch with the experimental data remains, showing that for rigid systems like indigo VE computations can be safely used in the first benchmark step in order to give an overall idea on the accuracy of different functionals. The relative ”stiffness” of new systems can be quantified in terms of the largest Huang-Rhys factors, which are easily available by performing VG computations with one functional only, as discussed for M2 and 1. The computed absorption maxima are also reflected in the colour prediction, shown in Figure 6 where VG spectra computed with different functionals are marked with lines corresponding to the predicted colours: RGB parameters of about 255:0:180 (pink) were obtained by CAM-B3LYP, M06-2X and ω-B97XD functionals, whereas the correct blue color (RGB: 0:~160:255) is forecasted by B3LYP and PBE0 functionals. As a matter of fact, these two latter functionals show the best agreement with respect to experiment within the whole UV-vis energy range, including the colour prediction.

For all other studied compounds the lowest bright excited electronic state is dominated by the HOMO-LUMO transition and is responsible for the predicted colour. The absorption maxima reported in Table 1 confirm the conclusions drawn for **1**. In all cases, CAM-B3LYP, M06-2X and ω-B97XD functionals yield λ_{max} lower than experiment by 70 to 55 nm, within VE and VG models, respectively. The apparently better agreement shown by VE TD-B3LYP computations with an average error of 11 nm (19 nm for PBE0) is overcome by VG computations which show an average accuracy of about 10 nm for both functionals. TD-B3LYP and TD-PBE0 computations predict correctly the relative shifts of absorbtion maxima between indigo derivatives, again with the VG results outperforming the basic VE model. The good agreement with experiment within the whole UV-vis energy range obtained with the TD-PBE0 and TD-B3LYP functionals is also confirmed for the other compounds, as shown for thioindigo (**2**) in Figure 7, further suggesting that both B3LYP and PBE0 are suitable for the studies of new indigo-derived dyes.

3.3 Toward indigo oligomers

Changes of optical properties of molecular dyes upon complexation and aggregation are of direct interest for the development of novel indigo-based materials. Here, we will consider an indigo dimer as a test case of larger macromolecular systems composed from indigo derivatives.

In order to obtain a reliable description of all weak intermolecular interactions, we have resorted to the B3LYP-D3 model[99, 100], which is able to deliver reliable structure, energetics and spectroscopic properties for hydrogen bonded and stacked stuctures[106, 107]. To optimize the dimer geometry, three, different guess-conformations have been used: one planar and symmetric with symmetry point group C_{2h}, another slightly distorted from planarity, and finally a stacked structure, with the two monomers placed in parallel planes (see Supplementary Information). The B3LYP-D3/CPCM computations starting from planar and nearly-planar conformations converged to the structure presented in Figure 8, characterised by nearly perpendicular indigo units. This structure obtained by considering dispersion interactions is significantly different from the nearly-planar geometries obtained at the B3LYP level in previous studies [25]. These difference clearly indicate that inclusion of dispersion interactions (here D3) is mandatory for obtaining reliable structural and energetic data. We note that planar structure can be a suitable model for the solid/cristal structures of high-density aggregates[75], but is not an equilibrium structure for the dimer in solution. Attempts to optimize the stacked structure didn't converge to an energy minimum, indicating that in lower concentrations stacked structures are less-likely. We can conclude that the equilibrium structure obtained from B3LYP-D3 computations, which has been confirmed as a minimum with all positive harmonic frequencies, is stabilized by both hydrogen-bond and dispersion interactions. The resulting geometry shows an intermolecular hydrogen-bond, shorter than the intramolecular one, partially justifying the great stability of indigo aggregates, while its bent shape is most likely stabilized by the interaction between delocalized electronic densities of the aromatic system. Only the 'bent' equilibrium structure reported in Figure 8 has been considered for spectra computations, which in view of the good performance of TD-B3LYP for indigo monomer and in order to facilitate comparison with previous studies[25] have been performed at the TD-B3LYP(D3)/SNSD/CPCM level. The presence of higher oligomers has been also postulated in Ref.[25]. Molecular dynamics computations including several indigo molecules together with explicit solvent molecules and proper boundary conditions could be performed for shedding light on this point, but this is well outside the purposes of the present investigation.

In the case of indigo there is only one bright excited state in the visible energy range, which is assigned to a HOMO$\rightarrow$LUMO transition. In the dimer the frontier MOs originate from those of the monomer, leading to two sets of nearly degenerate orbitals. These four orbitals are in the same energy range as HOMO and LUMO of the monomer, but give rise to several allowed transitions (see Figure 9). The four electronic transitions (S_1-S_4) present in the 600-800 nm spectral range and contributing to the overall colour of the compound are listed in Table 3. The corresponding ELD variations upon the electronic transition are localized over both moieties, but do not show inter-molecular charge transfer character: for purposes of illustration the ELD of the lowest $S_1 \leftarrow S_0$ transition is reported in Figure 10. All the

spectra contributing to the visible band (RGB:0:203:255), simulated at the vibronic VG/TD-B3LYP(D3)/SNSD/CPCM level are presented in Figure 11, while absorption maxima issuing from VE and VG computations are listed in Table 3. The most intense band in the dimer (S_4) shows at the VG level λ_{max}=610 nm, which agrees within 5 nm with that of the monomer. The remaining transitions are shifted towards lower energies, in particular the two lowest electronic transitions give rise to the broad shoulder in the red-energy wing of the spectrum, matching well the band at 700 nm observed experimentally at higher concentration of indigo[21]. It is noteworthy that our results show better agreement with experimental findings than previous theoretical investigation[25], performed at the VE/TD-B3LYP level for the planar structure of the dimer.

We recall that, in the VG approximation, the probability of specific electronic-vibrational transitions in the Franck-Condon regime are directly related to the Huang-Rhys (HR) factors [105], which are the squares of the components of the excited state gradient normalized with respect to the corresponding initial-state vibrational frequency. Detailed vibronic structures of all bands are presented in Figure 12, with the corresponding Huang-Rhys factors shown in Figure 13. On the overall for all four bands the same group of normal modes show the most significant contributions to the spectra. The ν_6, ν_{11} modes describe relative motions of rigid aromatic stuctures, while the others are related to the out-of-plane (ν_5 and ν_{13}) and in-plane (ν_8 and ν_{23}) ring deformations. The higher-frequency vibronic-active mode ν_{141} corresponds to the in-plane deformations within inter-molecular hydrogen bond, and can be closely related to the ν_{70} mode of the indigo monomer (see Figure 5). However, relative contributions vary between states as clearly represented by the largest Huang-Rhys factors: for S_1 the most intense transitions are related to the mode ν_{11}, for the S_2 to the mode ν_{13}, for S_3 to the mode ν_8, while for S_4 there is no dominant contribution. These findings clearly show that despite similarities each electronic transition has a distinct vibronic nature, of potential effects i.e. on energy transfer processes. Moreover, for all electronic transitions of the dimer the differences between VE and VG absorption maxima are larger than for **1** suggesting that both dispersion interaction and vibronic effects are important in studies of optical properties of indigoid oligomers.

4 Concluding remarks

The aim of this paper was twofold: from one side we want to investigate the spectroscopic characteristics of an important class of dyes in terms of stereo-electronic, vibronic, and environmental effects. Then, from a more general point of view, we want to present and validate the performances of our virtual multifrequency spectrometer (VMS) and of its new companion graphical user interface (VMS-Draw) for the study of large, possibly flexible molecular systems in their natural environment. For the specific case of indigo, we have convincingly demonstrated the limits of simplified molecular systems and of electronic computations neglecting vibronic couplings. As a matter of fact, careful selection of density functional, vibronic, and solvent models permitted to reach qualitative and quantitative vis-à-vis comparison between experimental and computed band positions and shapes. At the same time, the colour perceived by human eyes is correctly reproduced. Graphical and user friendly post- processing of the computed data has allowed us to fully analyze the results and to interpret them in terms of interactions between frontier orbitals and of leading

vibrational normal modes. Furthermore, the effect of inter-molecular interactions has been properly accounted for and interpreted also in terms of vibronic effects for indigo dimer. In a more general perspective, the definition of an integrated computational strategy and its implementation in a user friendly and robust package including powerful graphical facilities increases the possible role of computational spectroscopy studies to complement and interpret experimental spectroscopic outcomes in terms of suitable chemical models.

Supplementary Material

Refer to Web version on PubMed Central for supplementary material.

Acknowledgments

The research leading to these results has received funding from the European Union's Seventh Framework Programme (FP7/2007-2013) under the grant agreement N°ERC-2012-AdG-320951-DREAMS. The high performance computer facilities of the DREAMS center (http://dreams.sns.it) are acknowledged for providing computer resources. Alberto Baiardi is acknowledged for fruitful discussions and computations of Huang-Rhys factors.

References

1. Barone V, editorComputational Strategies for Spectroscopy, from Small Molecules to Nano Systems. John Wiley & Sons, Inc; Hoboken, New Jersey: 2011.
2. Kobayashi H, Ogawa M, Alford R, Choyke PL, Urano Y. Chem Rev. 2010; 110:2620. [PubMed: 20000749]
3. Kamerlin SCL, Warshel A. Phys Chem Chem Phys. 2011; 13:10401. [PubMed: 21526232]
4. Pedone A, Prampolini G, Monti S, Barone V. Chem Mater. 2011; 23:5016.
5. Curutchet C, Kongsted J, Munoz-Losa A, Hossein-Nejad H, Scholes GD, Mennucci B. J Am Chem Soc. 2011; 133:3078. [PubMed: 21322565]
6. König C, Neugebauer J. Chem Phys Chem. 2012; 13:386. [PubMed: 22287108]
7. Labat F, Le Bahers T, Ciofini I, Adamo C. Acc Chem Research. 2012; 45:1268. [PubMed: 22497694]
8. Prampolini G, Bellina F, Biczysko M, Cappelli C, Carta L, Lessi M, Pucci A, Ruggeri G, Barone V. Chem Eur J. 2013; 19:1996. [PubMed: 23280815]
9. Ribeiro AJM, Alberto ME, Ramos MJ, Fernandes PA, Russo N. Chem Eur J. 2013; 19:14081. [PubMed: 24014428]
10. Pedone A, Gambuzzi E, Barone V, Bonacchi S, Genovese D, Rampazzo E, Prodi L, Montalti M. Phys Chem Chem Phys. 2013; 15:12360. [PubMed: 23783271]
11. Dreuw A, Faraji S. Phys Chem Chem Phys. 2013; 15:19957. [PubMed: 24145385]
12. Boixel J, Guerchais V, Le Bozec H, Jacquemin D, Amar A, Boucekkine A, Colombo A, Dragonetti C, Marinotto D, Roberto D, Righetto S, et al. J Am Chem Soc. 2014; 136:5367. [PubMed: 24635126]
13. Laurent AD, Adamo C, Jacquemin D. Phys Chem Chem Phys. 2014; 16:14334. [PubMed: 24548975]
14. Goez A, Jacob CR, Neugebauer J. Comput Theoret Chem. 2014; 1040–1041:347.
15. Horch M, Hildebrandt P, Zebger I. Phys Chem Chem Phys. 2015; 17:18222. [PubMed: 26105154]
16. Imahori H, Umeyama T, Ito S. Acc Chem Research. 2009; 42:1809. [PubMed: 19408942]
17. Debije MG, Verbunt PPC. Advanced Energy Materials. 2012; 2:12.
18. van Sark WG. Renewable Energy. 2013; 49:207.
19. Reimers JR, Cai ZL, Kobayashi R, Ratsep M, Freiberg A, Krausz E. Sci Rep. 2013; 3:2761. [PubMed: 24067303]
20. Renger T, Muh F. Phys Chem Chem Phys. 2013; 15:3348. [PubMed: 23361062]

21. Miliani C, Romani A, Favaro G. Spectrochim Acta A. 1998; 54:581.
22. Pouli P, Selimis A, Georgiou S, Fotakis C. Acc Chem Research. 2010; 43:771. [PubMed: 20329718]
23. Fantacci S, Amat A, Sgamellotti A. Acc Chem Research. 2010; 43:802. [PubMed: 20429593]
24. Rosi F, Miliani C, Clementi C, Kahrim K, Presciutti F, Vagnini M, Manuali V, Daveri A, Cartechini L, Brunetti BG, Sgamellotti A. Applied Physics A. 2010; 100:613.
25. Amat A, Rosi F, Miliani C, Sgamellotti A, Fantacci S. J Molec Structure. 2011; 993:43.
26. Carta L, Biczysko M, Bloino J, Licari D, Barone V. Phys Chem Chem Phys. 2014:2897. [PubMed: 24424261]
27. Grunenberg J, editorComputational Spectroscopy: Methods, Experiments and Applications. Wiley-VCH Verlag GmbH & Co. KGaA; Weinheim, Germany: 2010.
28. Quack M, Merkt F, editorsHandbook of High-resolution Spectroscopy. John Wiley & Sons, Inc; 2011.
29. Barone V. Reference Module in Chemistry, Molecular Sciences and Chemical Engineering. Elsevier; 2014.
30. Burke K, Werschnik J, Gross EKU. J Chem Phys. 2005; 123:062206.
31. Casida ME. J Mol Struct Theochem. 2009; 914:3.
32. Jacquemin D, Wathelet V, Perpete EA, Adamo C. J Chem Theory Comput. 2009; 5:2420. [PubMed: 26616623]
33. Caricato M, Trucks GW, Frisch MJ, Wiberg KB. J Chem Theory Comput. 2010; 6:370. [PubMed: 26617296]
34. Isegawa M, Peverati R, Truhlar DG. J Chem Phys. 2012; 137 244104.
35. Furche F, Ahlrichs R. J Chem Phys. 2004; 121:12772.
36. Scalmani G, Frisch MJ, Mennucci B, Tomasi J, Cammi R, Barone V. J Chem Phys. 2006; 124:094107.
37. Liu J, Liang W. J Chem Phys. 2011; 135:184111. [PubMed: 22088056]
38. Liu J, Liang W. J Chem Phys. 2013; 138:024101. [PubMed: 23320662]
39. Barone V, Baiardi A, Biczysko M, Bloino J, Cappelli C, Lipparini F. Phys Chem Chem Phys. 2012; 14:12404. [PubMed: 22772710]
40. Biczysko M, Bloino J, Brancato G, Cacelli I, Cappelli C, Ferretti A, Lami A, Monti S, Pedone A, Prampolini G, Puzzarini C, et al. Theor Chem Acc. 2012; 131 1201/1.
41. Barone V, Biczysko M, Bloino J, Carta L, Pedone A. Comput Theoret Chem. 2014; 1037:35.
42. Vazart F, Latouche C, Bloino J, Barone V. Inorg Chem. 2015; 54:5588. [PubMed: 25992912]
43. Latouche C, Baiardi A, Barone V. J Phys Chem B. 2015; 119:7253. [PubMed: 25417746]
44. Chenu A, Christensson N, Kauffmann HF, Mancal T. Sci Rep. 2012; 3:2029.
45. Kolli A, O'Reilly EJ, Scholes GD, Olaya-Castro A. J Chem Phys. 2012; 137:174109. [PubMed: 23145719]
46. Barone V, Biczysko M, Borkowska-Panek M, Bloino J. ChemPhysChem. 2014; 15:3355. [PubMed: 25182331]
47. Etinski M, Petković M, Ristić MM, Marian CM. J Phys Chem B. 2015; 119:10156. [PubMed: 26189597]
48. Jacquemin D, Bremond E, Ciofini I, Adamo C. J Phys Chem Lett. 2012; 3:468. [PubMed: 26286048]
49. Santoro F, Improta R, Lami A, Bloino J, Barone V. Journal of Chemical Physics. 2007; 126:084509. [PubMed: 17343460]
50. Barone V, Bloino J, Biczysko M, Santoro F. J Chem Theory Comput. 2009; 5:540. [PubMed: 26610221]
51. Bloino J, Biczysko M, Santoro F, Barone V. J Chem Theory Comput. 2010; 6:1256.
52. Baiardi A, Bloino J, Barone V. J Chem Theory Comput. 2013; 9:4097. [PubMed: 26592403]
53. Petrenko T, Neese F. J Chem Phys. 2007; 127:164319. [PubMed: 17979350]
54. Petrenko T, Neese F. J Chem Phys. 2012; 137:234107. [PubMed: 23267471]

55. Dierksen M, Grimme S. J Chem Phys. 2004; 120:3544. [PubMed: 15268516]
56. Jankowiak HC, Stuber JL, Berger R. J Chem Phys. 2007; 127:234101. [PubMed: 18154369]
57. Dierksen M, Grimme S. J Chem Phys. 2005; 122:244101. [PubMed: 16035740]
58. Barone V, Baiardi A, Bloino J. Chirality. 2014; 26:588. [PubMed: 24839096]
59. Bloino J, Biczysko M, Barone V. J Chem Theory Comput. 2012; 8:1015. [PubMed: 26593363]
60. Bloino J, Barone V. J Chem Phys. 2012; 136:124108. [PubMed: 22462836]
61. Bloino J. J Phys Chem A. 2015; 119:5269. [PubMed: 25535769]
62. Baiardi A, Bloino J, Barone V. J Chem Phys. 2014; 141:114108. [PubMed: 25240346]
63. Licari D, Baiardi A, Biczysko M, Egidi F, Latouche C, Barone V. J Comput Chem. 2015; 36:321. [PubMed: 25408126]
64. Biczysko M, Bloino J, Santoro F, Barone V. Computational Strategies for Spectroscopy, from Small Molecules to Nano Systems. Barone V, editorWiley; Chichester: 2011. 361–443.
65. Lami A, Santoro F. Computational Strategies for Spectroscopy, from Small Molecules to Nano Systems. Barone V, editorWiley; Chichester: 2011. 475–516.
66. Clark RJ, Cooksey CJ, Daniels MA, Withnall R. Endeavour. 1993; 17:191.
67. Zollinger H. Color Chemistry. Syntheses, Properties and Application of Organic Dyes and Pigments. 3rd revised ed. Wiley-VCH; Weinheim, Germany: 2003.
68. Hunger K, editorIndustrial Dyes. Wiley-VCH Verlag GmbH & Co. KGaA; 2004.
69. Baeyer A, Drewsen V. Ber Deutsch Chem Ges. 1882; 15:2856.
70. Giustetto R, Llabrési Xamena FX, Ricchiardi G, Bordiga S, Damin A, Gobetto R, Chierotti MR. J Phys Chem B. 2005; 109:19360. [PubMed: 16853500]
71. Lüttke W, Hermann H, Klessinger M. Angew Chem Int Ed. 1966; 5:598.
72. Dähne S, Leupold D. Angew Chem Int Ed. 1966; 5:984.
73. Miehe G, Süsse P, Kupcik V, Egert E, Nieger M, Kunz G, Gerke R, Knieriem B, Niemeyer M, Lüttke W. Angew Chem Int Ed. 1991; 30:964.
74. Serrano-Andrés L, Roos BO. Chem Eur J. 1997; 3:717.
75. Jacquemin D, Preat J, Wathelet V, Perpète EA. J Chem Phys. 2006; 124 074104.
76. Jacquemin D, Preat J, Wathelet V, Fontaine M, Perpète EA. J Am Chem Soc. 2006; 128:2072. [PubMed: 16464110]
77. Perpète EA, Jacquemin D. J Mol Struct Theochem. 2009; 914:100.
78. Yamazaki S, Sobolewski AL, Domcke W. Phys Chem Chem Phys. 2011; 13:1618. [PubMed: 21152507]
79. Glowacki ED, Voss G, Sariciftci NS. Advanced Materials. 2013; 25:6783. [PubMed: 24151199]
80. Pina J, Seixas-de Melo JS, Eckert A, Scherf U. J Mater Chem A. 2015; 3:6373.
81. Fukumoto H, Nakajima H, Kojima T, Yamamoto T. Materials. 2014; 7:2030. [PubMed: 28788554]
82. Pramodini S, Poornesh P. Optics Laser Technology. 2014; 63:114.
83. Glowacki ED, Apaydin DH, Bozkurt Z, Monkowius U, Demirak K, Tordin E, Himmelsbach M, Schwarzinger C, Burian M, Lechner RT, Demitri N, et al. J Mater Chem C. 2014; 2:8089.
84. Robb MJ, Ku SY, Brunetti FG, Hawker CJ. J Polym Sci A Polym Chem. 2013; 51:1263.
85. Becke AD. J Chem Phys. 1993; 98:5648.
86. Yanai T, Tew DP, Handy NC. Chem Phys Lett. 2004; 393:51.
87. Zhao Y, Schults NE, Truhlar DG. J Chem Theory Comput. 2006; 2:364. [PubMed: 26626525]
88. Zhao Y, Truhlar DG. Theor Chem Acc. 2008; 120:215.
89. Chai JD, Head-Gordon M. Phys Chem Chem Phys. 2008; 10:6615. [PubMed: 18989472]
90. Adamo C, Barone V. J Chem Phys. 1999; 110:6158.
91. [last visited: 1 February 2015] Double and triple-ζ basis sets of sns family, are available in the download section. http://dreams.sns.it
92. Carnimeo I, Puzzarini C, Tasinato N, Stoppa P, Charmet AP, Biczysko M, Cappelli C, Barone V. J Chem Phys. 2013; 139:074310. [PubMed: 23968095]
93. Barone V, Biczysko M, Bloino J. Phys Chem Chem Phys. 2014; 16:1759. [PubMed: 24346191]

94. Bergner A, Dolg M, Kuchle W, Stoll H, Preuss H. Mol Phys. 1993; 80:1431.
95. Igelmann G, Stoll, Preuss H. Mol Phys. 1988; 65:1321.
96. Tomasi J, Mennucci B, Cammi R. Chem Rev. 2005; 105:2999. [PubMed: 16092826]
97. Cossi M, Scalmani G, Rega N, Barone V. J Comput Chem. 2003; 24:669. [PubMed: 12666158]
98. Baiardi A, Bloino J, Barone V. J Chem Theory Comput. 2015; 11:3267. [PubMed: 26575763]
99. Grimme S, Antony J, Ehrlich S, Krieg H. J Chem Phys. 2010; 132:154104. [PubMed: 20423165]
100. Grimme S. WIREs Comput Mol Sci. 2011; 1:211.
101. Cossi M, Barone V. J Chem Phys. 2001; 115:4708.
102. Beck ME. Int J Quantum Chem. 2005; 101:683.
103. Frisch MJ, Trucks GW, Schlegel HB, Scuseria GE, Robb MA, Cheeseman JR, Scalmani G, Barone V, Mennucci B, Petersson GA, Nakatsuji H. , et al. Gaussian 09 Revision D.01. gaussian Inc; Wallingford CT: 2009.
104. Cui G, Thiel W. Phys Chem Chem Phys. 2012; 14:12378. [PubMed: 22872211]
105. Huang K, Rhys A. Proc Roy Soc London A: Math, Phys Engin Sci. 1950; 204:406.
106. Fornaro T, Biczysko M, Monti S, Barone V. Phys Chem Chem Phys. 2014; 16:10112. [PubMed: 24531740]
107. Fornaro T, Carnimeo I, Biczysko M. J Phys Chem A. 2015; 119:5313. [PubMed: 25474755]
108. Haucke G, Seidel B, Graness A. J Photochem. 1987; 37:139.
109. Gerke R, Fitjer L, M P. Tetrahedron. 1999; 55:14429.
110. Wille E, Lüttke W. Angew Chem Int Ed. 1971; 10:803.
111. Haucke G, Graness G. Angew Chem Int Ed. 1995; 34:67.
112. Pummerer R, Marondel G. Chem Ber. 1960; 93:2834.
113. Clark RJH, Cooksey CJ. New J Chem. 1999; 23:323.
114. Sadler PW. J Org Chem. 1956; 21:316.

Europe PMC Funders Author Manuscripts

Europe PMC Funders Author Manuscripts

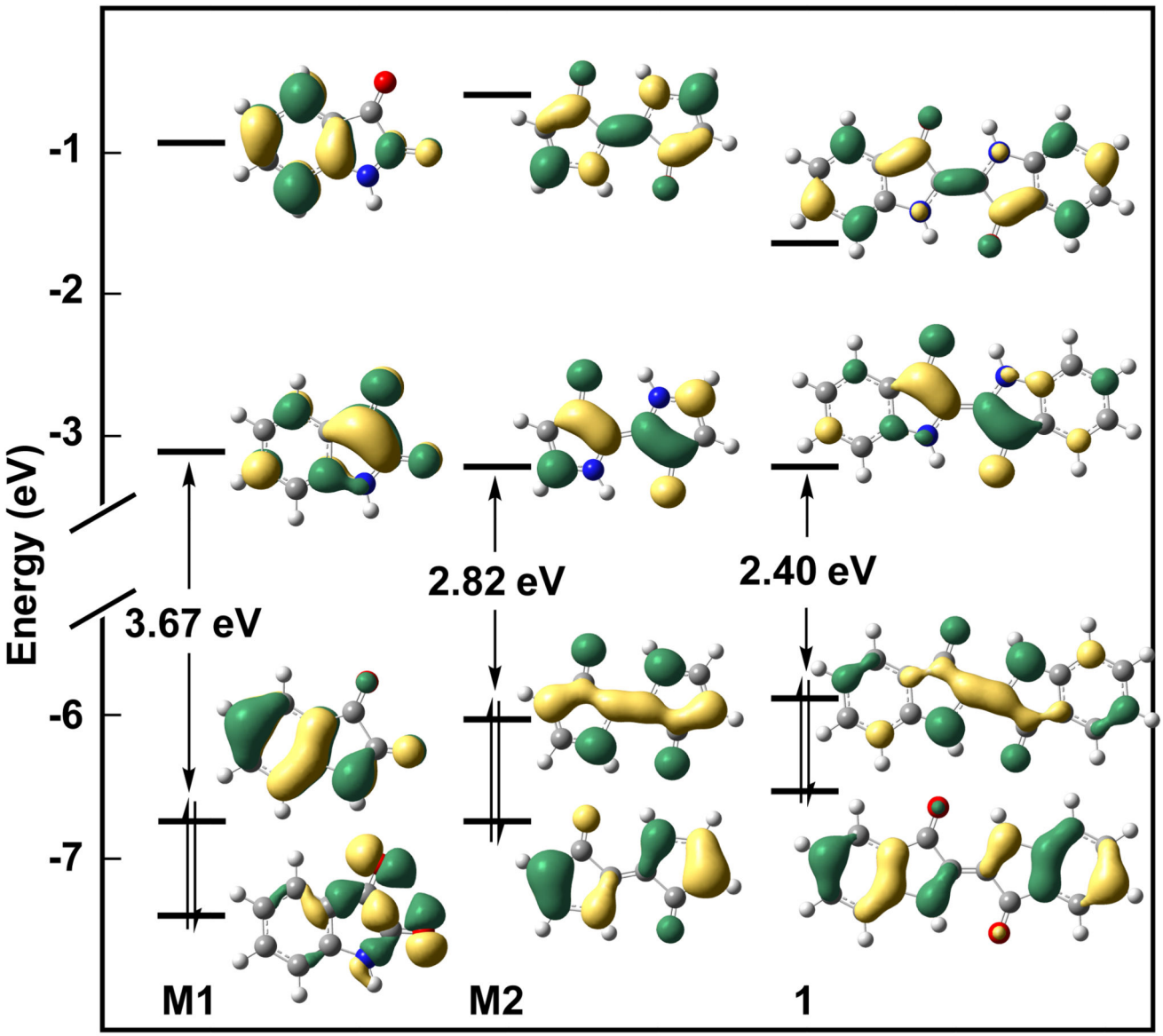

Fig. 1.
Frontier MOs diagrams of **M1**, **M2** and**1** computed at the B3LYP/SNSD/CPCM level.

Europe PMC Funders Author Manuscripts

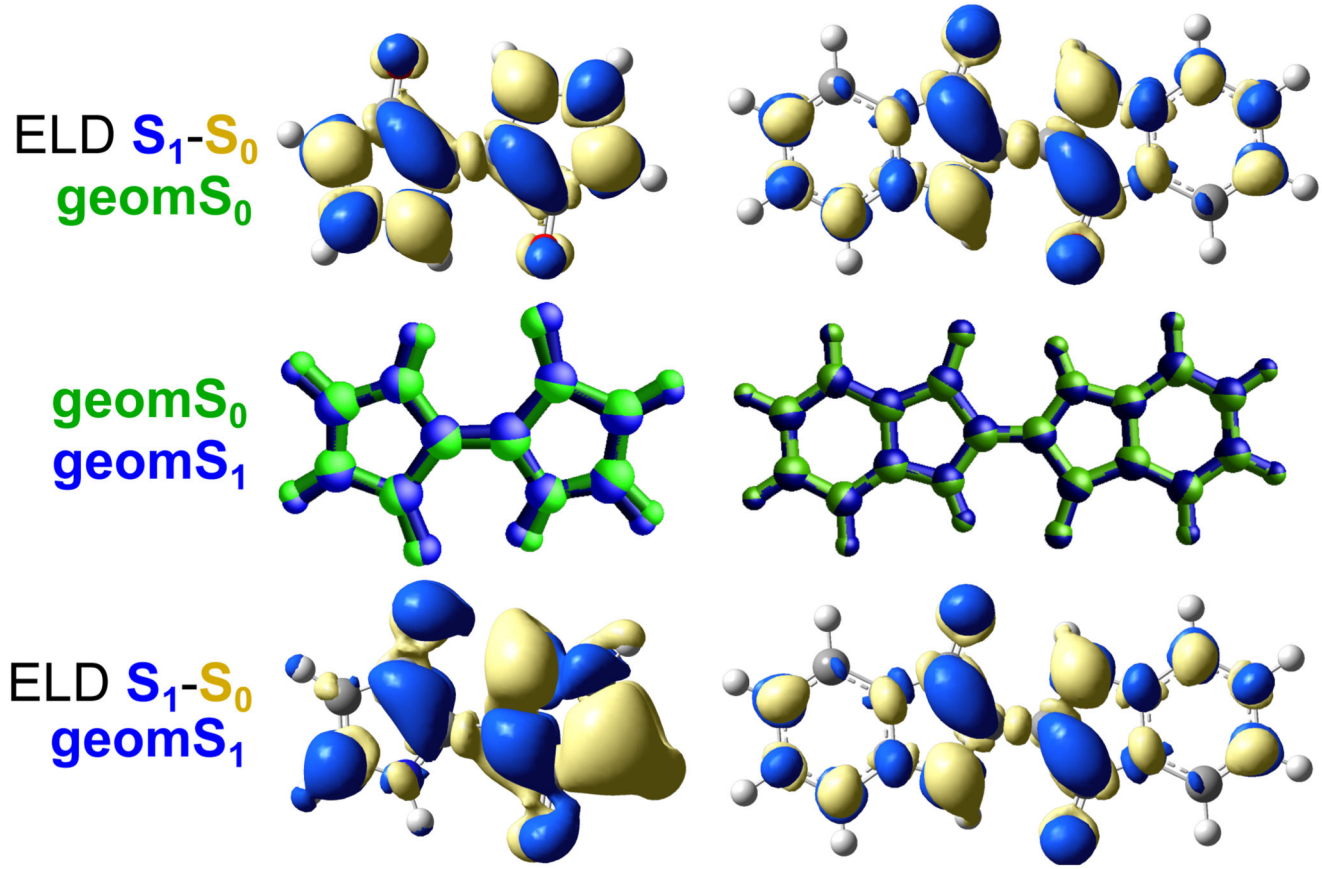

Fig. 2.

Changes of geometry structure and electron density upon electronic excitation for the **M2** and **1**. Superposition of the ground (green) and excited state (blue) equilibrium structures and plots of the difference in electron density (ELD) between the ground state and the first excited electronic state within vertical (geomS_0) and adiabatic (geomS_1) frameworks. The regions that have lost electron density as a result of transition are shown in yellow, whereas the blue regions have gained electron density. ELD densities were plotted with an isovalue threshold of 0.001.

Europe PMC Funders Author Manuscripts

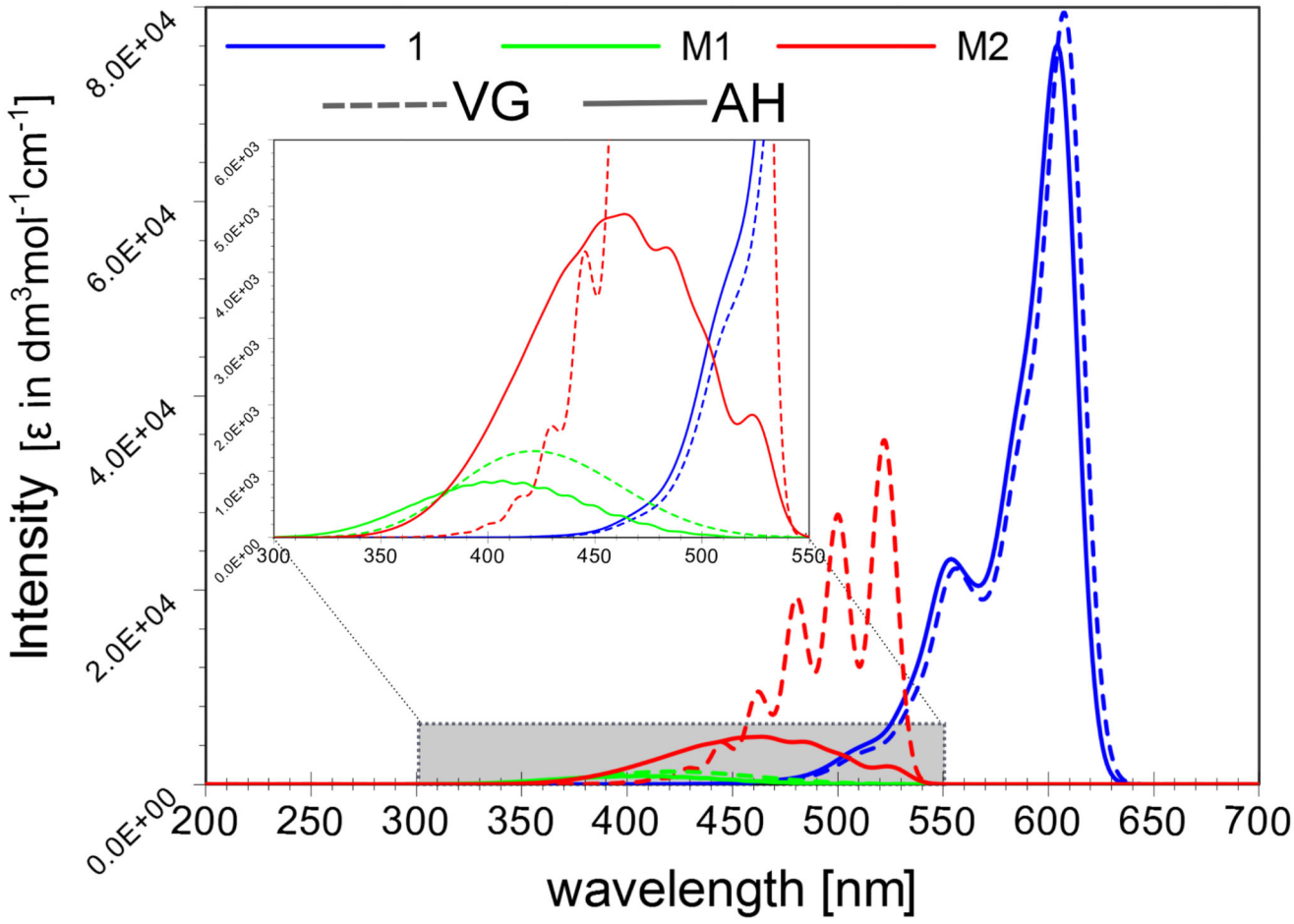

Fig. 3.

Theoretical absorption spectra for the fist bright electronic transition of **M1**, **M2** and **1**, simulated within Vertical-Gradient (VG) and Adiabatic-Hessian (AH) models. All spectra computed at the TD-PBE0/B3LYP/SNSD/CPCM model (see text for the details) and convoluted with the Gaussian distribution function of Half-Width at Half-Maximum (HWHM) of 250 cm^{-1}.

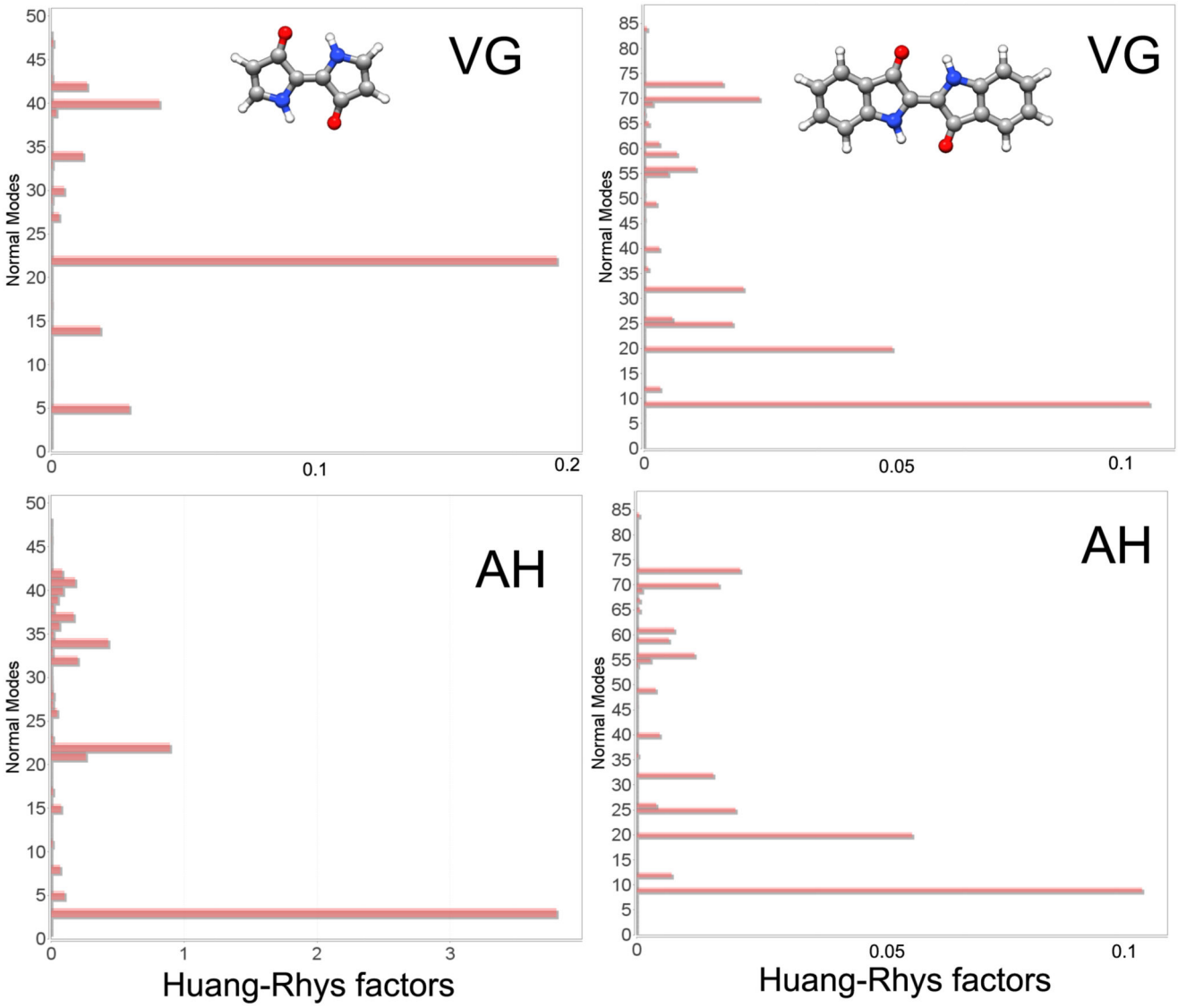

Fig. 4.

The Huang-Rhys factors of **M2**(left) and **1**(right), simulated within Vertical-Gradient (VG) and Adiabatic-Hessian (AH) models at the TD-B3LYP/SNSD/CPCM level.

Europe PMC Funders Author Manuscripts

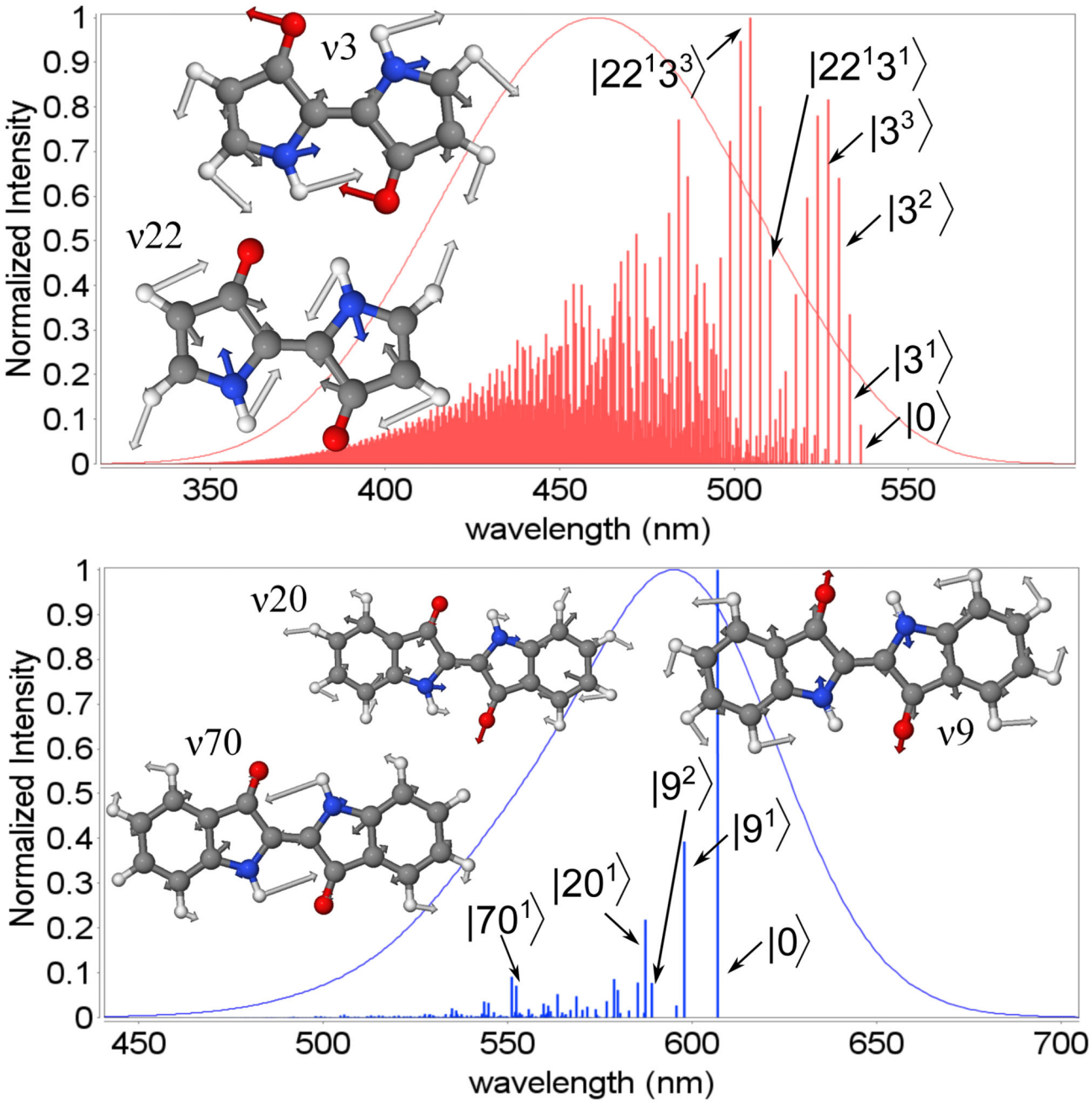

Fig. 5.

The $S_1 \leftarrow S_0$ spectra of **M2** (upper panel) and **1** (lower panel), simulated AH/TD-PBE0/B3LYP/SNSD/CPCM level along with the assignment of the selected most intense vibronic transitions (stick spectrum). The $|n^m>$ represents the final vibrational state of mode n with the number of quanta m in superscript. Normal modes in the ground and excited electronic states are equivalent (Duschinsky matrix $\mathbf{J} \simeq \mathbf{I}$). Spectrum band-shape obtained by convolution with the Gaussian distribution function of Half-Width at Half-Maximum (HWHM) of 750 cm^{-1} is also presented.

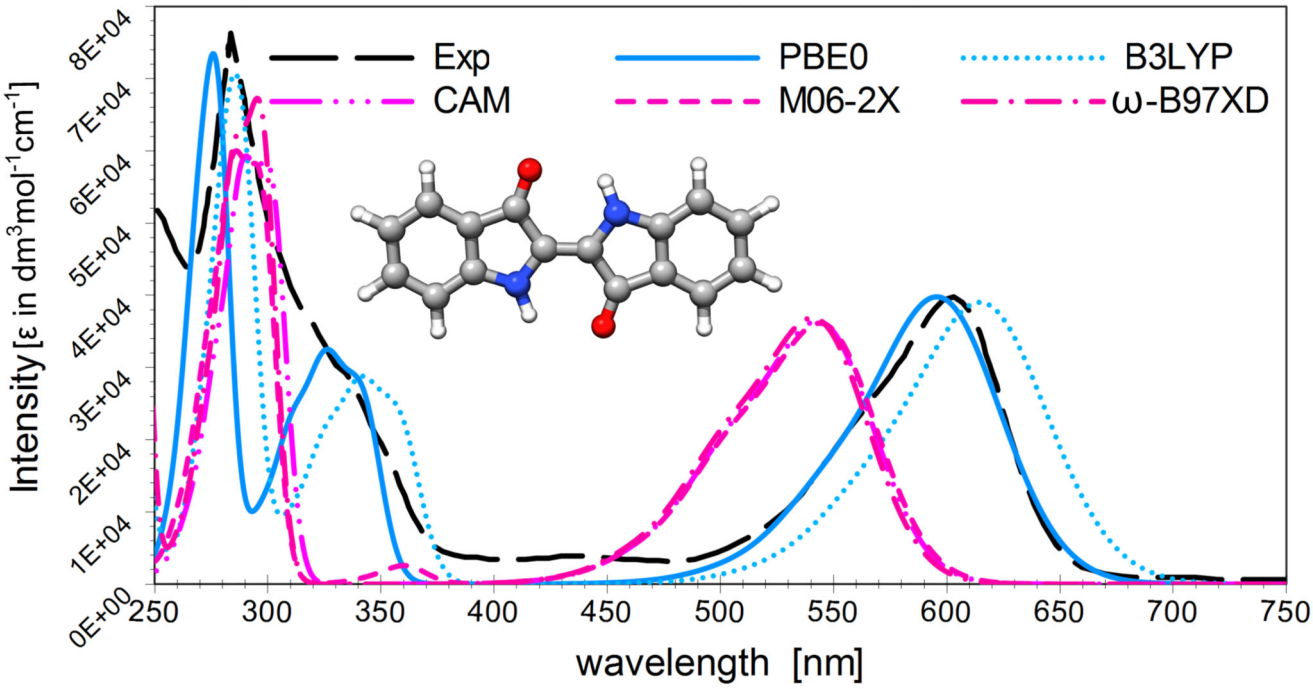

Fig. 6.

Absorption spectra of indigo in chloroform in a 250-750 nm range, computed at the VG level with different functionals and compared to its experimental counterpart[21]. Intensity of experimental spectrum is normalized to match the maximum of the theoretical VG/PBE0 one. Theoretical spectra are marked by lines with colour corresponding to the predicted theoretical RGB one.

Europe PMC Funders Author Manuscripts

Europe PMC Funders Author Manuscripts

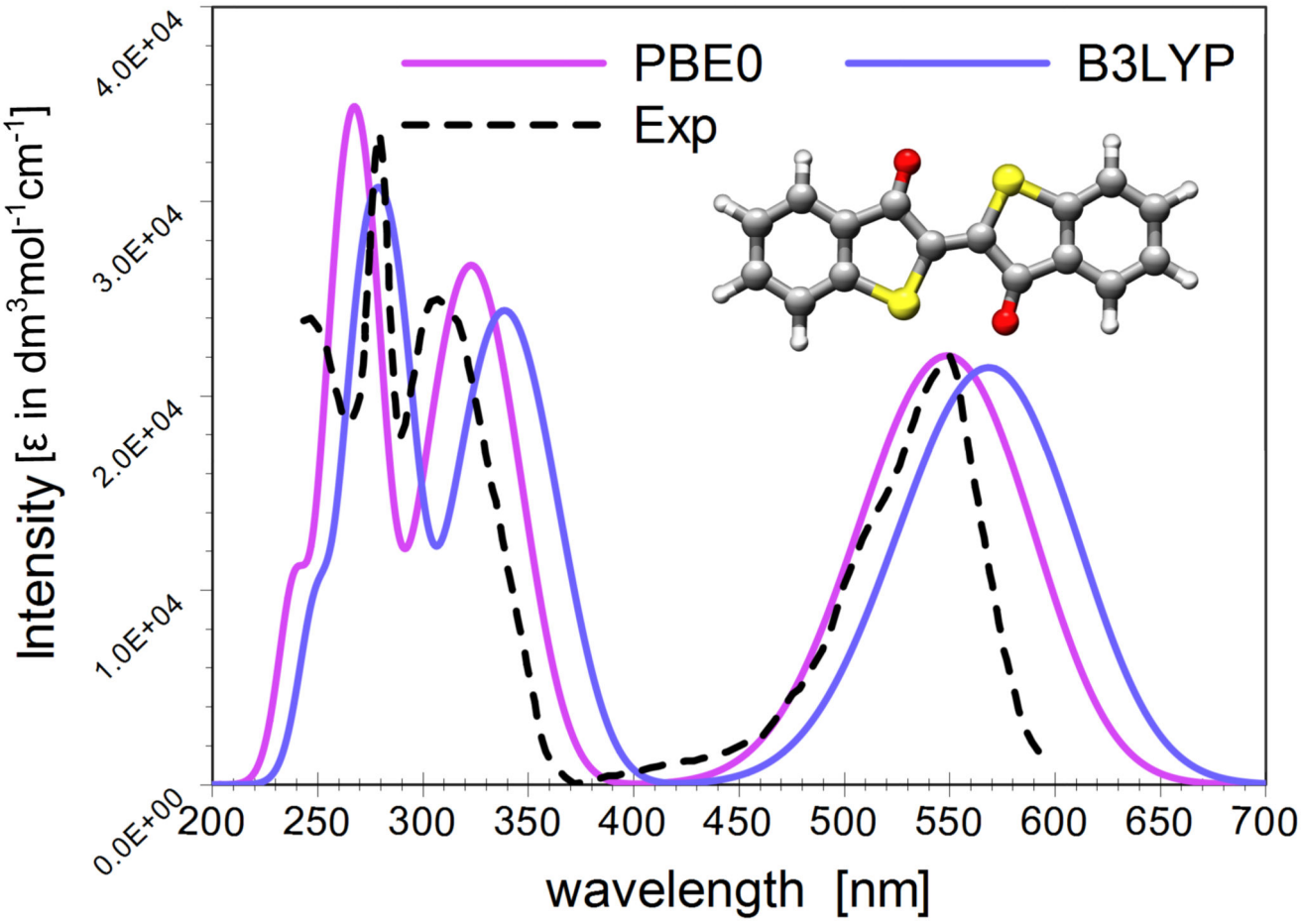

Fig. 7.

Absorption spectra of thioindigo in chloroform in a 250-750 nm range, computed at the VG/TD-PBE0 and VG/TD-B3LYP levels and compared to its experimental counterpart[112]. Intensity of experimental spectrum is normalized to match the maximum of the theoretical one. Theoretical spectra are marked by line with colour corresponding to the predicted theoretical RGB one.

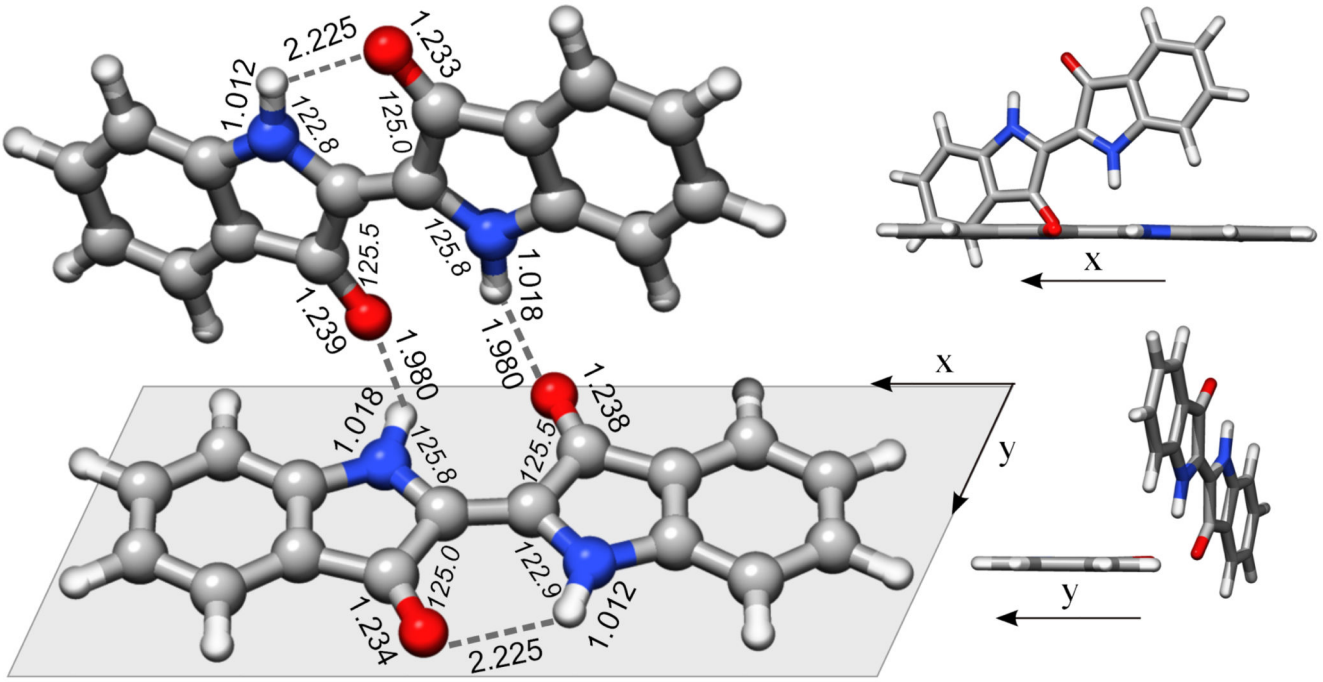

Fig. 8.

Equilibrium structure of indigo dimer computed at the B3LYP-D3/SNSD/CPCM level. Selected bond lengths (in Å) and angles (in degrees) are reported along with the side views.

Europe PMC Funders Author Manuscripts

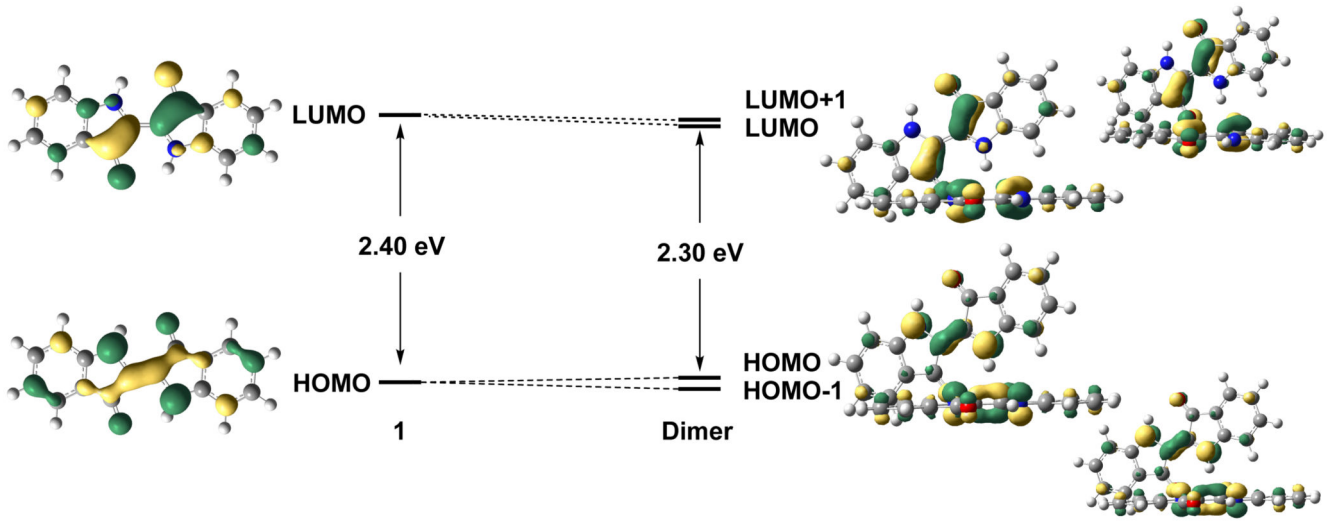

Fig. 9.

Frontier MOs of indigo monomer and dimer. Contributions to the one electron transitions of the dimer computed at the B3LYP-D3/SNSD/CPCM level.

Europe PMC Funders Author Manuscripts

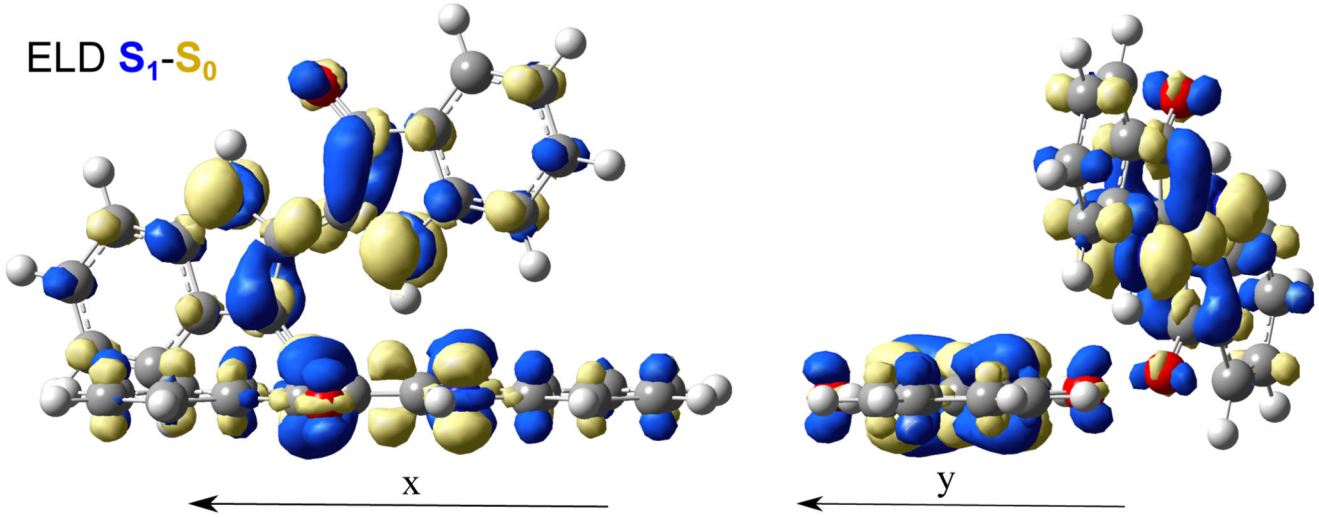

Fig. 10.

Changes in electronic density (ELD) for $S_1 \leftarrow S_0$ electronic transitions of indigo dimer, computed at the TD-B3LYP/SNSD/CPCM level for the ground state equilibrium structure optimized at the B3LYP-D3/SNSD/CPCM level. The regions, which have lost electron density as a result of the transition, are shown in bright yellow, whereas the darker blue regions gained electron density. ELD densities were evaluated with an isovalue threshold of 0.001. For the side views description see Figure 8.

Europe PMC Funders Author Manuscripts

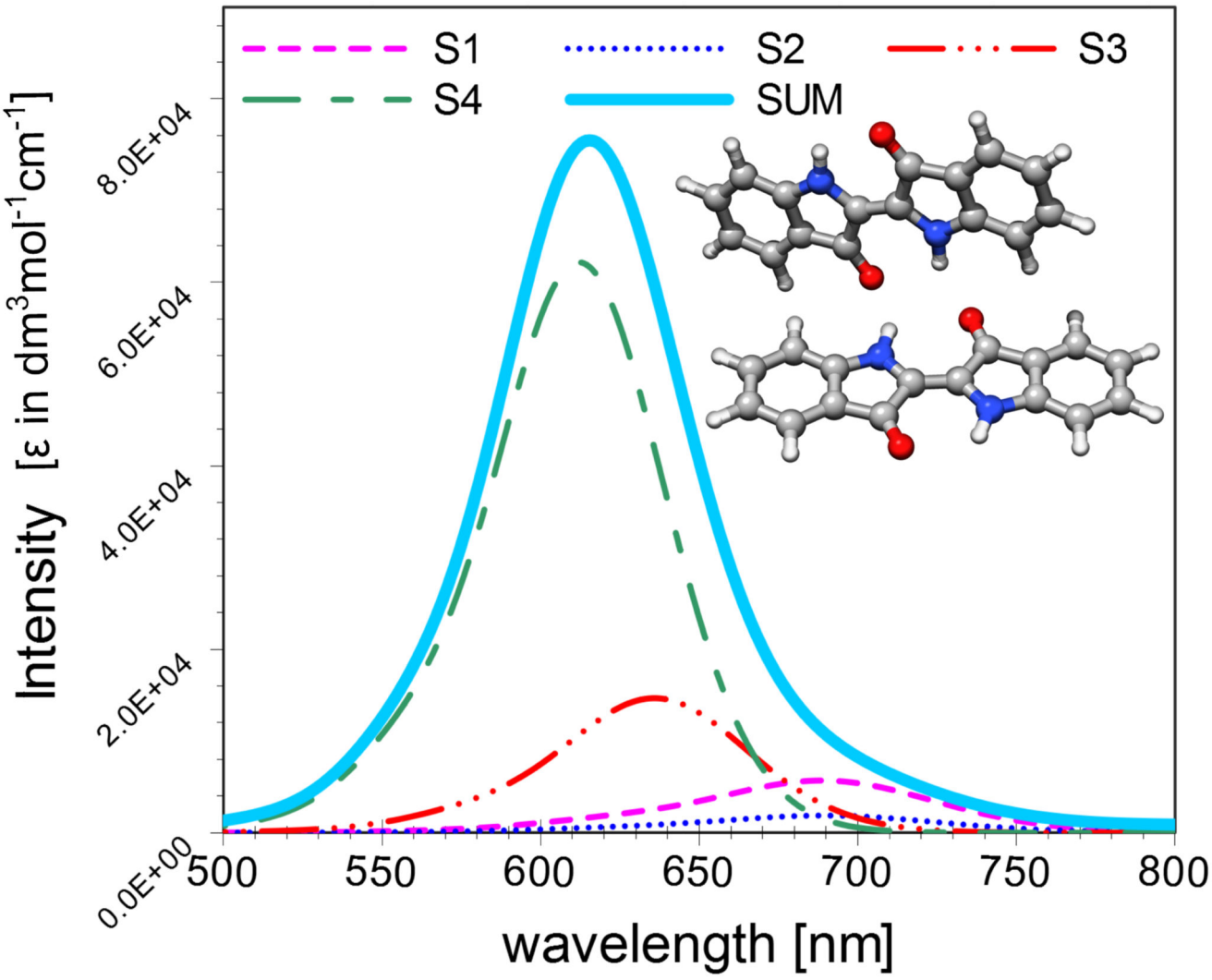

Fig. 11.

Spectra of indigo dimer in the 500-800 nm energy range simulated at the VG level with the B3LYP functional. Single electronic transitions are convoluted with the Gaussian distribution function with the HWHM of 750 cm^{-1}. Total sum spectrum is marked by line with colour corresponding to the predicted theoretical RGB one (0:203:255).

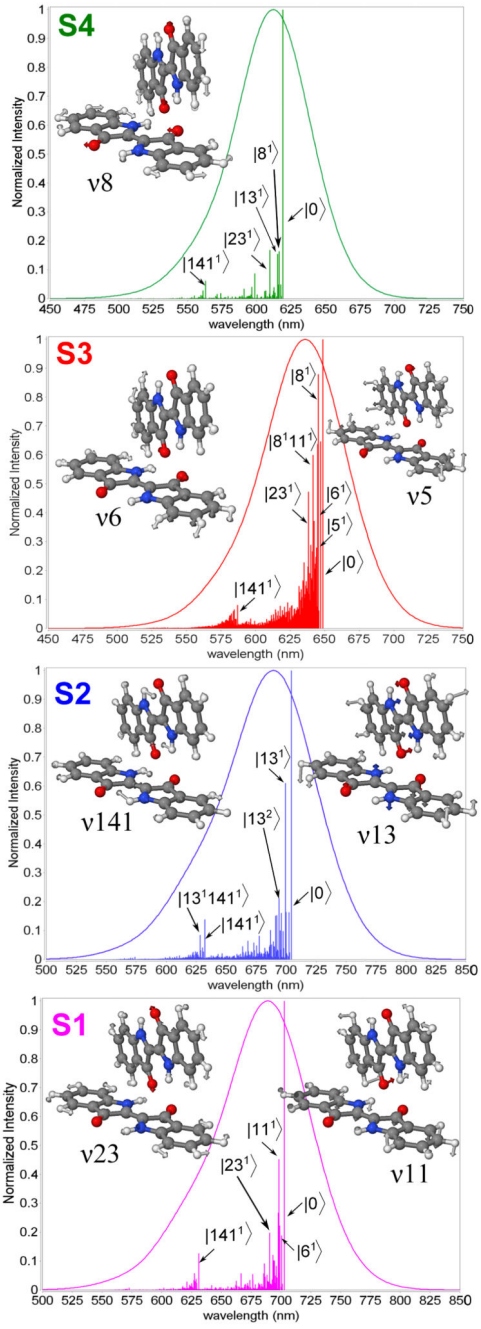

Fig. 12.

The single electronic transition spectra of indigo dimer, simulated at the VG/TD-B3LYP-D3/SNSD/CPCM level along with the assignment of the selected most intense vibronic transitions (stick spectrum). The $|n^m>$ represents the final vibrational state of mode n with the number of quanta m in superscript. Normal modes correspond to the ground electronic state. Spectrum band-shape obtained by convolution with the Gaussian distribution function of Half-Width at Half-Maximum (HWHM) of 750 cm^{-1} is also presented.

Europe PMC Funders Author Manuscripts

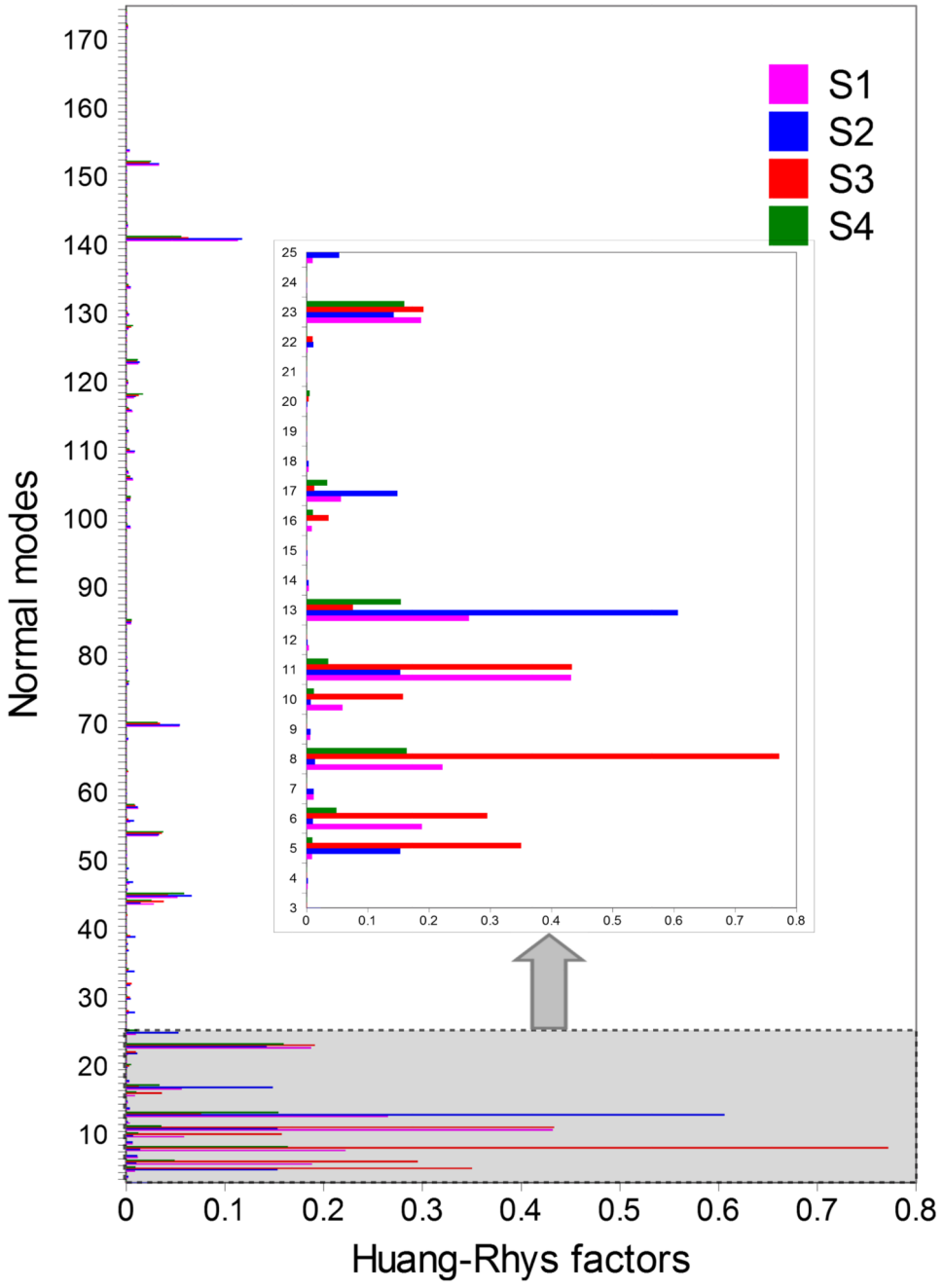

Fig. 13.

The Huang-Rhys factors for single electronic transition spectra of indigo dimer, simulated at the VG/TD-B3LYP-D3/SNSD/CPCM level. For normal modes description see Figure 12.

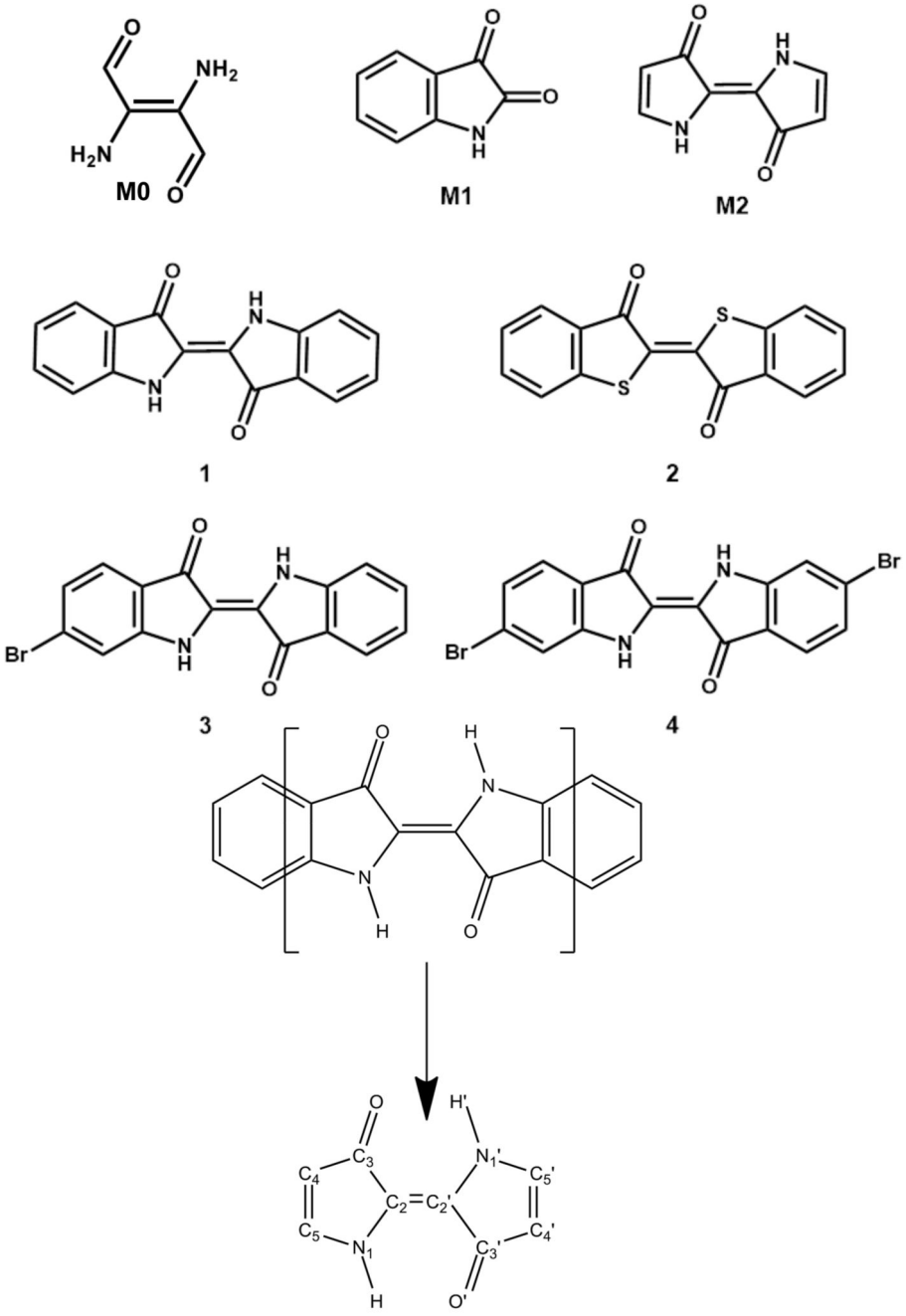

Scheme 1.

Scheme of the indigo reduced models (**M0-2**) and indigo-derivatives (**1-4**) skeletal formula, along with the atom numbering of the main chromophoric unit.

Europe PMC Funders Author Manuscripts

Europe PMC Funders Author Manuscripts

Table 1

Experimental and theoretical λ_{max} (in nm) for the first bright excited state of compounds **M1-2** and **1-4**, computed by vertical energy (VE) and vibronic (VG) models at TD-B3LYP, TD-CAMB3LYP, TD-PBE0, TD-M06-2X and TD-ωB97XD levels, in conjunction with SNSD basis set and CPCM(chloroform). The computed oscillator strengths (f) are also listed.

compound	Exp.	B3LYP			PBE0			ω-B97XD			CAM-B3LYP			M06-2X		
	λ_{max}	λ_{max}		f	λ_{max}		f	λ_{max}		f	λ_{max}		f	λ_{max}		f
		VE	VG[a]		VE	VG[a]		VE	VG[a]		VE	VG[a]		VE	VG[a]	
M1	415[b]	430	437	0.025	413	420	0.027	374	380	0.034	374	381	0.034	368	373	0.035
M2	528[c]	504	533	0.207	490	520	0.216	460	493	0.255	460	494	0.253	466	500	0.252
1	604[d]	599	615	0.337	580	599	0.352	522	541	0.392	524	543	0.391	524	544	0.389
2	550[e]	559	569	0.254	540	549	0.273	467	475	0.309	469	477	0.305	468	474	0.304
3	601[f]	594	608	0.265	579	592	0.377	517	530	0.416	520	532	0.410	520	534	0.410
4	590[g]	587	601	0.383	572	585	0.406	525	538	0.448	515	527	0.437	514	528	0.439
MAE[h]		11	12		19	6		71	55		71	56		72	56	

[a] Vibronic spectra convoluted with the Gaussian distribution function with HWHM of 750 cm^{-1}. For **M1** and **M2** results from vibronic AH computations.

[b] in chloroform[108].

[c] in ethanol for 3,3',4,4'-tetramethylbispyrroleindigo[67].

[d] in chloroform[73], absorption maxima in ethanol[109] and tetrachloroethane[110, 111] are 606 nm and 605 nm, respectively.

[e] in chloroform[112].

[f] in tetrachloroethane[113].

[g] in tetrachloroethane[114].

[h] Mean absolute error (MAE) with respect to the experiment.

Europe PMC Funders Author Manuscripts

Table 2

Selected equilibrium geometry parameters of **M2** and **1** in the ground (S_0) and the first excited electronic state (S_1).

Compound	Bond length [Å]	S_0	S_1	$\Delta(S_1\text{-}S_0)$
Indigo (**1**)	N-H	1.013	1.018	0.005
	N-C2	1.379	1.378	-0.001
	C2-C2’	1.362	1.386	0.024
	C2-C3	1.492	1.465	-0.028
	C3-O	1.235	1.251	0.016
	O-H’	2.295	2.284	-0.011
M2	N-H	1.012	1.011	-0.001
	N’-H’	1.012	1.030	0.018
	N-C2	1.378	1.365	-0.013
	N’-C2’	1.378	1.427	0.049
	C2-C2’	1.354	1.388	0.034
	C2-C3	1.504	1.478	-0.026
	C2’-C3’	1.504	1.423	-0.081
	C3-O	1.239	1.263	0.025
	C3’-O’	1.239	1.250	0.011
	O-H’	2.331	2.700	0.369
	O’-H	2.331	1.978	-0.352

Europe PMC Funders Author Manuscripts

Table 3

Theoretical λ_{max} (in nm) for the first four excited states of **1** dimer, computed by vertical energy (VE) and vibronic (VG) models at TD-B3LYP levels, in conjunction with SNSD basis set and CPCM (chloroform). The computed oscillator strengths (f) are also listed.

State	Molecular Orbitals	λ_{max}		f
		VE	VG[a]	
S_1	HOMO-1→LUMO(32%)+HOMO→LUMO+1(68%)	660	690	0.002
S_2	HOMO-1→LUMO+1(36%)+HOMO→LUMO(64%)	660	690	0.007
S_3	HOMO-1→LUMO(68%)-HOMO→LUMO+1(32%)	593	637	0.084
S_4	HOMO-1→LUMO+1(64%)-HOMO→LUMO(36%)	565	610	0.334

[a]Vibronic spectra convoluted with the Gaussian distribution function with HWHM of 750 cm^{-1}.